IOP PUBLISHING JOURNAL OF PHYSICS D: APPLIED PHYSICS

J. Phys. D: Appl. Phys. **41** (2008) 074026 (8pp) doi:10.1088/0022-3727/41/7/074026

Characterization of deformation field in plane-strain indentation of metals

T G Murthy, C Huang and S Chandrasekar[1]

Center for Materials Processing and Tribology, School of Industrial Engineering, Purdue University, West Lafayette, IN 47907-2023, USA

E-mail: chandy@ecn.purdue.edu

Received 3 October 2007, in final form 5 December 2007
Published 12 March 2008
Online at stacks.iop.org/JPhysD/41/074026

Abstract

A study has been made of the deformation field in plane-strain indentation of metals with a flat punch. Deformation field parameters such as velocity and strain rate have been measured using the technique of particle image velocimetry. For this purpose, images of the indentation region were recorded *in situ* during the deformation process, and motion of 'asperities' specially introduced onto a side of the sample being indented was analysed. The velocity and strain rate fields in and around the indentation zone were obtained from an analysis of the asperity motions. The measurements have shown, among other things, the presence of a dead metal zone underneath the indenter, the formation and evolution of regions of intense strain rates or shear bands and a linear variation of the strain rate with indentation speed. Many of the characteristics of the deformation field, e.g. slip lines and dead metal zone, compare favourably with those inferred from classical solutions for this indentation problem. Extensions of the technique for the study of strain field around indentations and deformation in plane-strain indentation by wedges and cylinders are discussed.

(Some figures in this article are in colour only in the electronic version)

1. Introduction

Quasi-static indentation is now a widely used technique for studying mechanical properties of solids such as hardness, flow stress and elastic modulii (Tabor 1951, 1996, Chaudhri and Enomoto 1996). Indentation tests are also being used to explore phenomena such as creep and strain gradient plasticity. In interpreting data from these applications of quasi-static indentation, concepts of representative strain, strain rate and strain gradient have been used, even though the theoretical underpinnings of these concepts have been less than rigorously established. A better understanding and clarification of these concepts could potentially be realized if a general experimental method was available for studying deformation field parameters such as velocity of material flow, strain rate and strain in indentation. Such measurements should also enable an assessment of various models of indentation based on data that are far more detailed than what are typically available in ensemble measurements of load–displacement and hardness, leading to possible improvements in measurement of the mechanical properties. It is in this context that this exploratory study to develop a direct method for measuring parameters of the indentation deformation field has been undertaken. While the experimental method is described for the model system of plane-strain indentation of a semi-infinite solid by a flat punch, it is equally applicable to other plane-strain configurations such as wedge and cylinder indentation.

Measurements of the strain distribution in the indentation region have generally relied on post-indentation observation of 'microstructure features' associated with the deformation or on correlation of hardness with strain. The extent of the plastic zone around indentations in brass was characterized by Samuels and Mulhearn (1957) using a metallographic etching technique that was sensitive to the level of strain in the material. The spatial resolution of this technique is determined by the resolution of the microstructures induced at varying levels of strain, and the technique is limited to selecting materials that exhibit this strain sensitivity of microstructure. In this context, it is worth noting that the recrystallization microstructure characteristic of a specific level of strain may be used to highlight the plastic zone around a spherical indentation, see

[1] Author to whom any correspondence should be addressed.

the beautiful series of micrographs presented in Hanemann and Schrader (1927). Nadai (1931) has also presented a similar recrystallization micrograph indicative of a characteristic level of strain around a flat punch indenter.

Direct measurements of deformation around an indenter have been carried out by Hill *et al* (1947), Nye (1947), Atkins and Tabor (1965) and Yew and Goldsmith (1964), using the 'split specimen' approach. In this approach, the specimen being indented is split into two halves and grids are inscribed on each of the surfaces of the solid to be conjoined. The two halves are clamped to create a monolithic specimen. The distortion of the grids is examined after the indentation by separating the halves. While this approach provides some insight into material flow, accurate measurement of strain rate and strain parameters is not feasible due to deformation of the split halves in the third dimension. Another important disadvantage of this method is that the deformation of a split specimen is likely different from that of a whole (un-split) specimen (Chaudhri 1993).

Chaudhri (1993) developed an elegant variation of the use of grids to measure strain distribution by indenting mild steel specimens which had inherent pearlite 'stringers' aligned perpendicular to the indentation direction. The stringers served as markers, intrinsic internal grids, whose distortion could be measured to estimate the strain. The directionally aligned pearlite stringers were a consequence of the macroscopic texture resulting from a drawing process used to produce the steel. While this offers a direct method for measurement of the strain, it is restricted to materials with resolvable pearlitic (e.g. steels) or similar aligned microstructure features. The spatial resolution of the measurements is determined by the size and interlamellar spacing of the pearlite stringers. This approach has also provided qualitative insights into the friction condition prevalent at the indenter–specimen contact, based on consideration of the nature of the stringer distortions (cutting or bending of the stringers).

In a follow-on study, Chaudhri (1996) characterized the strain distribution around a large spherical indentation in copper by studying the extent of hardening produced by the indentation. This was done by carrying out Vickers hardness measurements along a median plane section of the spherical indentation and correlating these hardness values with strain, using the hardness of copper specimens strained to different levels in uniaxial compression. The measurements gave an estimate of the plastic strain around the indentation, with the maximum plastic strain recorded below the indentation along the load axis.

The studies of Chaudhri (1993, 1996) have by far provided the best characterization to date of the strain field around an indentation. It should be noted that none of the aforementioned studies estimated the strain rate in the indentation zone.

The technique of particle image velocimetry (PIV) offers scope for direct *in situ* measurement of various parameters of the deformation field (velocity, strain rate, strain) in indentation. This technique relies on the analysis of image sequences of the indentation region taken during indentation of a suitably prepared specimen. Noteworthy in this regard are the studies by White and Bolton (2004) and O'Loughlin *et al* (2003) of deep indentation (piling) and shallow indentation (shallow footings) in sands; and studies of a special type of 'sliding wedge indentation' of metals by Lee *et al* (2004, 2006). In the studies on sand, the inherent texture of the sand particles was used to track the motion of these particles during the deformation process using the PIV technique. A direct measure of the displacement field around the indenter tip (pile tip) in deep and shallow indentation was obtained, along with the strain field in and around the indentation region.

This study builds on the prior work of Lee *et al* (2004, 2006) on measurement of strain field in sliding indentation of metals, and describes an adaptation of the PIV technique to directly determine the velocity and strain rate fields in plane-strain indentation by a flat punch. Efficacy, accuracy and precision of this method are comparable to that of local instrumentation. The results are compared with classical solutions of velocity and strain rate fields for punch indentation, providing a preliminary evaluation of a versatile experimental technique.

2. Particle image velocimetry

PIV is an optical measurement technique that has been widely used since the early 1980s to obtain velocity fields in macroscopic fluid flows (Adrian 1991). In this technique, particles (or tracers) are injected into the fluid and tracked to determine the velocity field. Recently, this technique has been adapted to study deformation, namely, velocity, strain rate and strain, in severe plastic deformation of metals (Lee *et al* 2004, 2006) and indentation of soils (White and Bolton 2004). A variant of a prior approach (Lee *et al* 2004, 2006) is used here to measure parameters of the deformation field (velocity, strain rate) in plastic indentation of a solid by a punch under plane strain conditions.

Figure 1 shows a schematic of the experimental arrangement for plane-strain indentation of a solid by a rectangular punch. An inset in this figure also shows the width and depth of indentation used in the analysis in the following sections. One surface (side face) of the model material system, lead, is prepared for imaging by abrasion. When the abraded side face of the lead sample is illuminated, an optical 'texture' is formed, due to scattering of light from the crests and troughs of the 'asperities' of the lead surface as shown in figure 2. A region of interest around the indenter is imaged using a charge-coupled device (CCD) camera attached to an optical microscope. The camera is stationary with respect to the region of interest. As the indentation progresses, the asperities in the region of interest are displaced, this displacement being captured by the CCD camera. A sequence of images from the region of interest, all with the same exposure time, is thus obtained for the analysis; this approach is generally called multiple frame, single exposure PIV.

For the analysis, two images from a sequence taken at a certain time interval apart are considered. Each image is divided into a grid of a desired size as shown in figure 2. An interrogation window, typically larger than the grid size is then specified. A single grid element is chosen for the

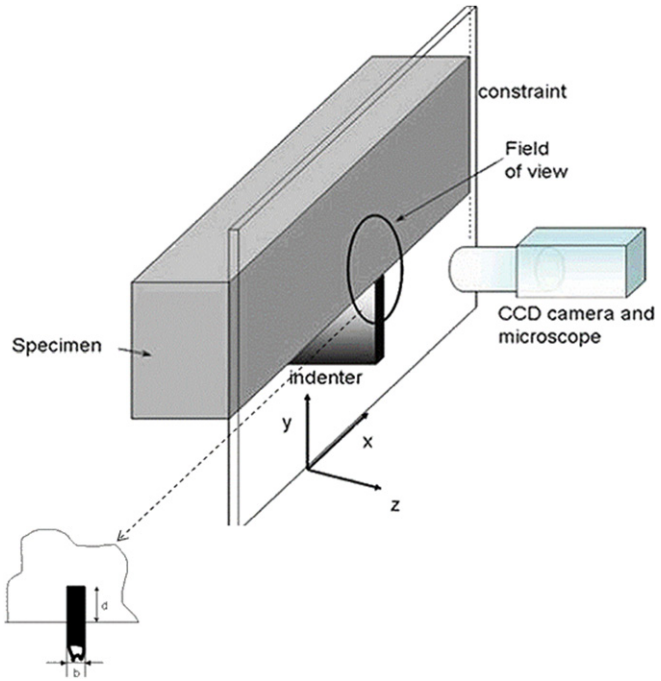

Figure 1. Schematic of experimental set up for plane-strain indentation. The indenter is placed on the fixed base of an universal testing machine while the lead sample is mounted on the moving cross-head. The sample is moved vertically downward at a pre-set speed. Inset shows depth of indentation (d) and contact length (b) of the indenter.

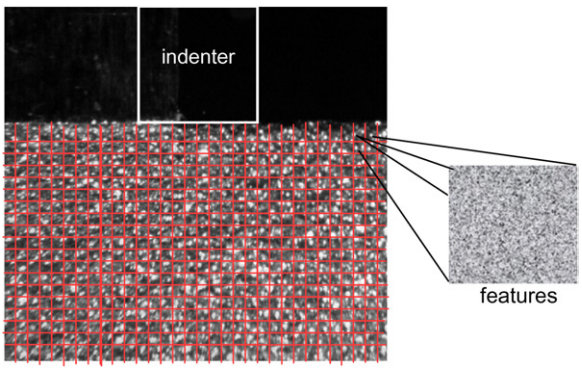

Figure 2. Indentation region showing lead sample just brought into contact with high speed steel indenter. The abraded surface of the sample, when illuminated by white light, shows a 'texture' that is used in the PIV. Also shown is an artificial grid of desired size that is superposed onto the image for the PIV analysis.

analysis in the first image. This single grid element is overlaid and traversed throughout the specified interrogation window in the second image of the image pair. A 'degree of match' is assessed through the PIV algorithm and the best match is located by using a cross-correlation function (Nguyen and Wereley 2002). The peak of the cross correlation indicates the displacement vector for the asperities of a particular grid. The calculation time is reduced by applying a fast Fourier transform to the region of interest. This procedure of finding the displacement vector is repeated for the entire set of grid elements, thus producing a displacement field for the whole region being imaged, in this case the region around the indenter. The analysis is continued by substituting the second image of the image pair with subsequent images from the image sequence. Thus an overall averaged displacement field is obtained for the quasi-static indentation using the entire sequence of images. The time interval between images and the evolving displacement field provide a map of the velocity in the deformation process.

White *et al* (2003) investigated the effect of interrogation patch size and grid size on the accuracy and precision of PIV measurements. Although they utilized the PIV for measuring deformation fields and gradients in soils, elements of their analysis are equally well applicable for plastic flow fields in metals. Their work suggests the selection of an optimized interrogation patch size: a larger interrogation window offers improved precision, whereas a smaller interrogation window allows for greater detail to be resolved in regions of higher strain gradient. In this study, an interrogation window size of approximately 3 times the grid size was chosen for all of the PIV analysis. White *et al* (2003) used a photogrammetric calibration procedure for conversion between object space and image space. This transformation also accounts for noise and errors due to non-coplanarity of object and image planes, radial and tangential lens distortion of the CCD camera, and refraction due to the glass block used here as a constraint to ensure plane-strain conditions (figure 1). This kind of transformation would be essential if the field of view is large. However, due to the relatively small area of interest observed (5 mm × 5 mm) and imaged in this experiment, a linear scaling approach was used to convert the object space to the image space.

The linear transformation factor, i.e. magnification of the lens, was verified against a calibration stage of a micrometer. The size of the grid measured through imaging and transformation matched well with the actual calibrated grid. A part of the indenter was also imaged throughout the deformation process to provide a constant frame of reference.

3. Strain and strain rate estimation

The velocities obtained from the PIV analysis can be used to calculate the strain rate and the strain in and around the indentation. The PIV analysis provides a grid of velocity vectors over the field of view. The strain rate components are estimated as (Thomsen *et al* 1965, Lee *et al* 2004, 2006)

$$\dot{\varepsilon}_{xx} = \frac{\partial u}{\partial x},$$
$$\dot{\varepsilon}_{yy} = \frac{\partial v}{\partial y},$$
$$\dot{\gamma} = 2\dot{\varepsilon}_{xy} = \frac{\partial v}{\partial x} + \frac{\partial u}{\partial y}, \tag{1}$$
$$\dot{\varepsilon}_{\text{eff}} = \sqrt{\frac{4}{9}\left(\frac{1}{2}\left[(\dot{\varepsilon}_{xx} - \dot{\varepsilon}_{yy})^2 + \dot{\varepsilon}_{xx}^2 + \dot{\varepsilon}_{yy}^2\right] + \frac{3}{4}\dot{\gamma}^2\right)},$$

where u and v are the velocity components in the x and y directions. The strain rate components are calculated numerically using the velocity values at the discrete grid points. To calculate the incremental strain imposed in a material

volume as it traverses a grid element, the strain rates and velocities at the grid points are needed. The velocity and the strain rate in a grid element are assumed to be constant. Then, the product of the strain rate and time required to traverse a particular grid element (this time is calculated from the velocity at the grid point) is the incremental strain imposed in that particular grid element. Furthermore, by integrating the strain rate field in this manner along particle trajectories, the cumulative strain at different locations in the sample during the indentation can be obtained (Lee *et al* 2006).

4. Experimental

A series of punch indentations was performed on a lead block, 127 mm long, 25.4 mm wide and 25.4 mm high, that was mounted onto the moving cross-head of a tension/compression test machine (MTS Qtest/50LP, 50 kN). The lead surface being indented was prepared by machining. The surface roughness ($R_a \sim 1\,\mu$m) was much smaller than the indentation size. The stationary indenter was a flat punch ($2.54 \times 25.4 \times 5.4\,\text{mm}^3$) machined out of high speed steel. The experimental arrangement is shown in figure 1. The contact length of the indenter and the depth of indentation are labelled as (b) and (d), respectively, in the figure. The indenter was attached to the fixed cross-head (base) of the machine and approximately in the middle of the lead block, with the indenter extending across the entire width of the lead block. The height of the lead sample (25.4 mm), as measured in the direction of indentation, was sufficiently large compared with the contact length of the indenter ($b = 2.54$ mm) so as to endure deformation typical of a semi-infinite medium. An optically smooth glass block was clamped to the indenter base and kept lightly pressed and aligned against the lead sample so as to minimize any transverse flow of material in the direction of the sample width (Lee *et al* 2004, 2006). The glass block remained in contact with the entire side face of the lead block throughout the indentation process thus ensuring a plane-strain condition during the indentation. The region in and around the indentation was imaged for the PIV analysis. In this experimental arrangement, the sample material sweeps through the region being imaged while the indenter is stationary.

A CCD based high speed camera (Nikon-Optiphot, Nikon Inc, Mellville, NY) coupled to an optical microscope was used for observation and imaging. The microscope allowed for magnifications of up to 200 times. A white light source was used for the illumination. The typical framing rate was 30 images per second. The spatial resolution in measurement of the velocity and strain rate field is $\sim 30\,\mu$m, for the smallest field of view used in the experiments. The indentation was carried out under displacement control with the cross-head of the MTS machine being moved at a constant velocity in the range 1–8.5 mm s^{-1}. The indenter load was measured using a 50 kN load cell attached to the cross-head of the testing machine.

Commercially pure lead (99.8% purity with 0.2% trace elements, McMaster-Carr, Elmhurst, IL, USA) was chosen as the model sample material, because its mechanical behaviour resembles that of a perfectly plastic solid at room temperature. The Vickers hardness of the lead was measured as 7.1 kg mm^{-2} (10 g indentation load).

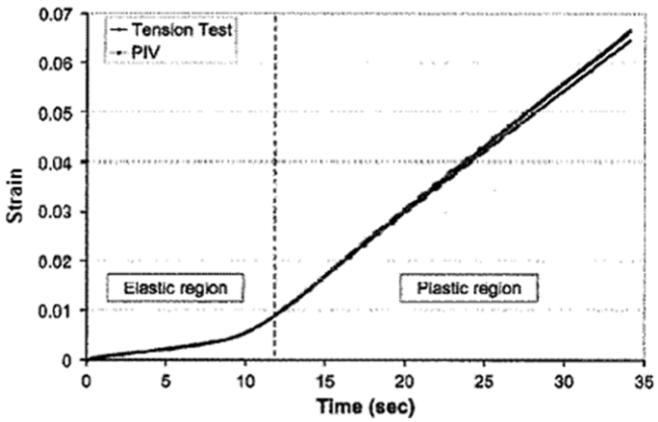

Figure 3. Comparison of strains in plate sample stressed in uniaxial tension calculated from PIV and directly measured by an extensometer attached to the test sample.

5. Calibration

The uniform deformation in a uniaxial extension test was used to calibrate the accuracy of the PIV for studying deformation. Ideally, all the displacement vectors in this uniform deformation field would be identical in both magnitude and direction enabling also identification of regions of noise and spurious displacement vectors in the CCD images. The PIV-based measurements of displacement and strain were compared with the analogous values measured directly using an extensometer. The two sets of values were in agreement to within 5% when measuring uniaxial tensile strains of up to 0.05, as seen in figure 3, which encompasses both the elastic and the plastic regimes of deformation strain. Strain components in different sample orientations were also estimated using the PIV by rotating the sample images that were recorded. These measurements again showed a good match with estimates obtained from the extensometer measurement and suitably transformed by the rotation.

Additional *in situ* calibration of the PIV was done by measuring the velocity of the lead sample subjected to cross-head motion without indentation. Images of the sample side face were obtained while it was moved at a pre-set velocity. The velocities measured by the PIV technique were compared against the pre-set velocities, that is, cross-head velocities; once again excellent agreement was noted. The precision and accuracy of the velocity field were further verified by studying the deformation when the same image was copied multiple times to form a sequence. When the PIV was applied to this image sequence, a value of zero was obtained for the velocity field everywhere, with minimal noise, serving as a consistency check.

6. Results

Figure 4 shows a typical sequence of images of the indentation recorded by the CCD-based imaging system that clearly

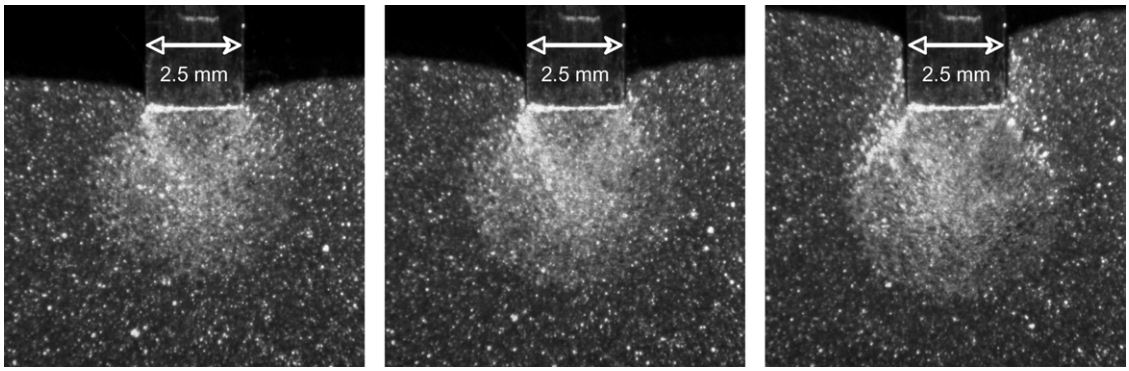

Figure 4. Sequence of images in indentation with a flat punch. The images are shown inverted with respect to the actual experimental configuration with the indenter on top for ease of understanding. A region of deformation, partially spherical, may be seen under the indenter. The images are taken at a low magnification so as to show a larger field of view.

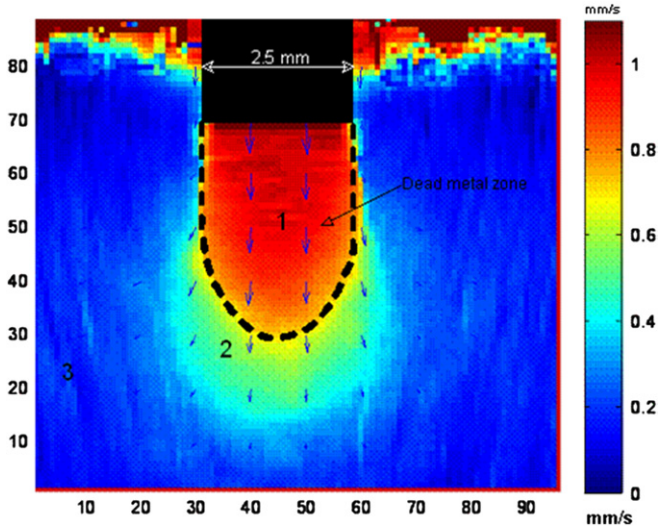

Figure 5. Velocity field from PIV analysis for a large field of view. This field provides a qualitative description of material flow around the indenter. The indenter velocity is 1 mm s^{-1} in the downward direction and the velocity scale is in mm s^{-1}. The region with velocity approximately equal to 1 mm s^{-1} under the indenter indicates a dead metal zone (region 1), since the material here is essentially stationary with respect to the indenter. Note that while in the experiment the indenter is stationary and the sample moves with respect to the indenter, in this and other figures the velocities are shown assuming the indenter is moving down with respect to a stationary sample, as in a typical indentation test.

highlight the indentation process. Even though the indenter was stationary with respect to the sample in the experiments, the results such as in figure 4 are presented such that the indenter is shown moving vertically downwards at a uniform velocity and the sample is stationary. This is to facilitate easy identification and comparison with quasi-static indentation in practice. A spherical cap of deformed material is evident in the image sequence in figure 4. Asperities are clearly seen on the side of the sample, which are used in the PIV analysis.

Figure 5 shows a map of the velocities obtained from the PIV analysis of image sequences such as these shown in figure 4. The velocity contours are plotted for a large field of view (low magnification). The velocity of the material immediately underlying the indenter and in contact with it is seen to be nearly constant and equal to the velocity of indentation (1 mm s^{-1}). Consequently, this material is stationary with respect to the indenter and corresponds to a dead metal zone (region 1) that acts as an extension of the indenter. The dead metal zone is seen to resemble a hemispherically capped rectangle in figure 5 and intersects the bottom face of the indenter at nearly right angles. The velocity field is approximately symmetrical with respect to the indenter mid-plane (axis) as is expected. The velocity of material flow decreases from a value of $\sim$1 mm s^{-1} near the indenter (region 1), which is the velocity of indentation, to about 0.6 mm s^{-1} (60% of the indentation velocity) in region 2 beyond the dashed line in the figure. Finally at distances sufficiently far away from the indenter, in region 3, the velocity of the material is essentially zero. The velocities very close to the indented (free) surface of the sample are not analysed here because of uncertainties arising from material pile-up. These three regions are delineated in figure 5 with velocity vectors imprinted at select locations. The maximum extent of the dead metal zone underneath the indenter is about 1.4 times the width of the indenter. Although the large field of view shown in figures 4 and 5 is ideal for obtaining a qualitative description of the velocity field, the resolution is insufficient to characterize strain rate, shear localization (velocity discontinuity) and evolution of strain rate in the indentation zone.

To better characterize the deformation, the indentation zone was observed at a higher magnification by reducing the field of view to a region encompassing only one-half of the indenter and the surrounding material. Symmetry considerations dictate that the other half of the deformation field is similar and indeed this was noted in the experiments. The velocity and strain rate fields derived from this observation are shown in figures 6(*a*) and (*b*), respectively. The three regions of distinct velocity identified in the low magnification view (figure 5) are also identified here, with region 1 corresponding to a velocity of about 1 mm s^{-1} (dead metal zone), region 2 corresponding to a velocity of about 0.6 mm s^{-1} and region 3 to velocities of $\sim$0.2 mm s^{-1} decaying down to zero farther away. Velocity vectors at

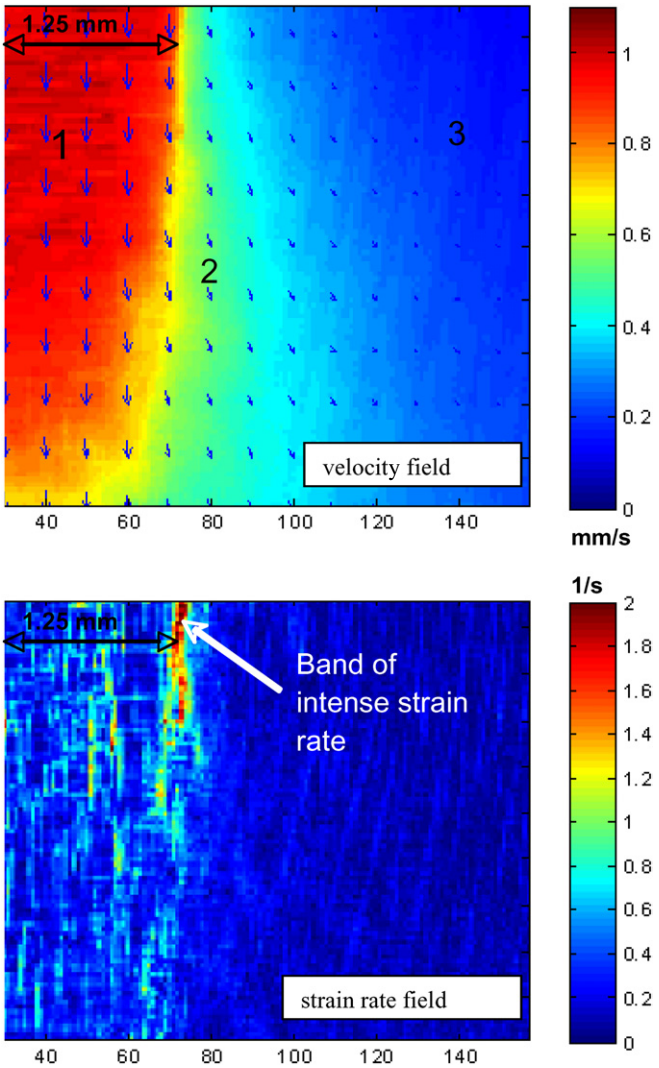

Figure 6. (*a*) Velocity and (*b*) strain rate fields obtained from PIV analysis of images. Only one half of the indentation region and the surrounding indentation are shown. The velocity field map shows vectors whose lengths are indicative of the magnitude of the velocities.

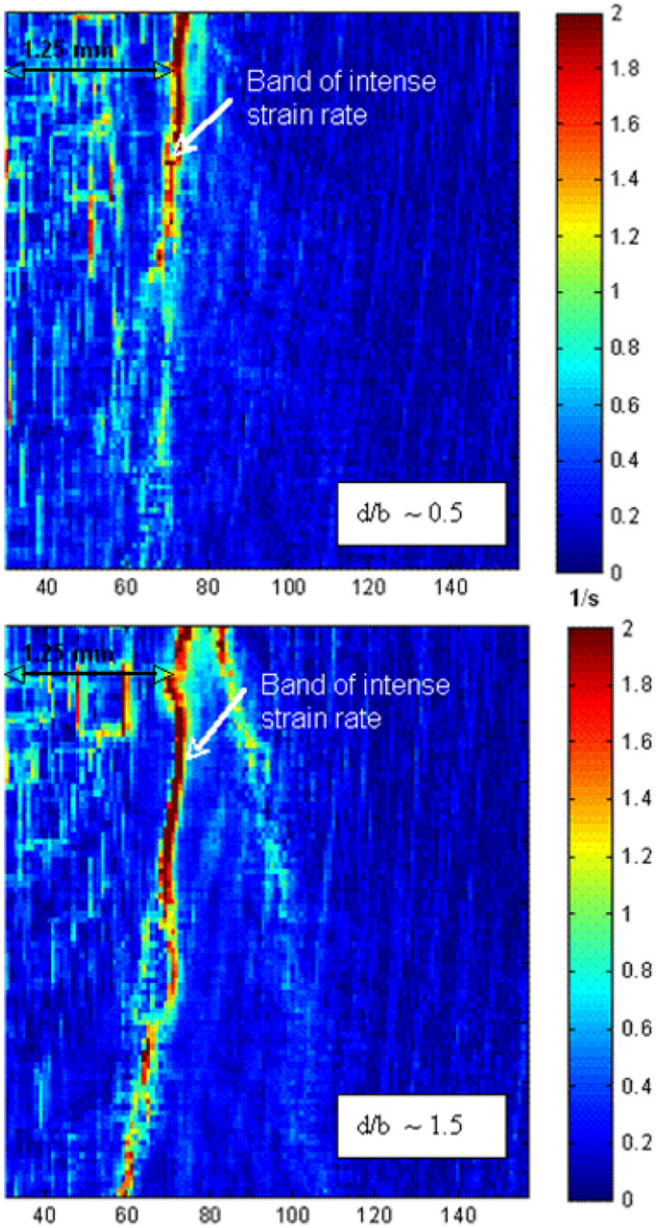

Figure 7. Strain rate field at two different depths of indenter penetration. The shear band and its propagation into the solid are seen to increase with increasing depth of indentation. Note also the development of a second shear band in (*b*). (*a*) Shallow and (*b*) deeper.

select locations in the indentation region are also shown in figure 6(*a*). It was observed in the images recorded at a higher magnification that the indenter did not penetrate the asperities introduced on the side surface. Rather, as the indentation progressed, these asperities were displaced below the indenter indicating a sticking type of friction condition at the indenter–sample interface. A similar observation has been made by Chaudhri (1993) in wedge indentation of mild steel, based on the deformation of the pearlite stringers.

The strain rate field in figure 6(*b*) shows the presence of a region of intense strain rate, see marked region, with an effective strain rate magnitude of $\sim$1.8 s^{-1} at the corner of the indenter. This region of intense strain rate will, henceforth, be referred to as a shear band. The shear band begins to develop almost at right angles to the bottom face of the indenter.

As the indenter penetrates deeper into the sample, with progression of the indentation, the velocity and strain rate fields become better defined with much sharper transitions in the magnitudes of the velocities, and continued development of the shear band. This may be seen in figure 7 which shows the strain rate field at two different stages of the indentation process. The maximum value of the strain rate at the corner of the indenter continues to remain at $\sim$1.8 s^{-1} with progression of the indentation, but the shear band curves towards the axis of the indenter. Figure 7(*b*) also shows the formation of another shear band at the corner of the indenter that curves away from the axis of the indenter.

The variation of the strain rate with indentation velocity was studied using indentation velocities of 1, 5 and 8.5 mm s^{-1}. The velocity of material flow and strain rates in the deformation zone were found to scale approximately linearly with the indentation velocity. The maximum strain rate, typically recorded in the shear band emanating from a corner of the

indenter, was ∼1.8 times the indentation velocity (in mm s^{-1}) in magnitude.

7. Discussion

A study has been made of the velocity and strain rate fields in indentation of an elastic–perfectly plastic solid by a flat punch. The technique of PIV has been applied to image sequences recorded of the indentation region, from which the strain rate and velocity have been estimated at different locations. The velocity field has highlighted three distinct regions of velocity (figures 5 and 6)—a dead metal zone underneath the indenter wherein the material is essentially stationary with respect to the indenter; a central fan shaped zone of different velocity adjoining this dead metal zone; and a region of very low velocity far away from the indenter. The strain rate field has revealed the formation and propagation of shear bands from the corners of the indenter (figure 7). The main shear band propagates towards the axis of the indenter. As indentation progresses, a second shear band is observed that propagates away from the axis of the indenter (figure 7(*b*)).

It is instructive to compare these results with some of the classical solutions for the plane-strain punch indentation problem. Two of the principal features of the measured deformation field are the dead metal zones, and the shear bands seen in the strain rate field (figure 7) which are the analogue of slip lines. The observed dead metal zones are compatible with both Prandtl's slip line field solution and laminar flow resulting from dislocation loop punching (Johnson *et al* 1970, Friedel 1964). Preliminary analysis of the measured deformation field data suggests qualitative agreement with Prandtl's slip line field. Quantitative and more concrete comparisons between the experimental results and classical solutions will soon be possible when the hodograph and slip line field are constructed from the experimentally observed deformation field. Such a comparison will facilitate a more rigorous description of the deformation field around an indenter, while also providing reliable values of the magnitudes of strain.

While the strain rate magnitudes along the shear bands scale as ∼1.8 times the indentation velocity (in mm s^{-1}), this prediction cannot be directly compared with slip line field theory wherein the shear band appears as a region of velocity discontinuity. However, the linear scaling of the strain rate with indentation velocity observed in the experiment is consistent with general considerations of strain rate inferred from plasticity analysis. Lastly, the velocity of indentation did not affect the development and shape of the dead metal zone, or that of the shear bands, as is to be expected from theory for a rate insensitive plastic solid.

The experiments have also provided important insights into the formation and propagation of the shear bands. The shear bands are quite 'narrow', originating at the corners of the indenter and then propagating into the bulk of the solid from these locations (figure 7). As the indentation progresses, the shear bands become better defined as seen in the strain rate fields of figure 7. An interesting feature pertaining to shear bands is the occurrence of a main shear band, followed by a secondary one which forms at a subsequent stage of the indentation. The main band curves towards the axis of the indenter and demarcates the boundary of the dead metal zone (region 1 in figure 7) while the secondary one curves away from the axis. The strain rate values in both the primary and the secondary shear bands are similar and their propagation in figure 7(*b*) is analogous to that seen in slip line fields. At higher depths of indentation, $d/b > 1.75$, it became difficult to track the motion of particles in and around the indentation zone due to the larger deformations imposed in these regions. This precluded a determination of whether shear bands, in addition to the main and secondary ones discussed above, form. Also, an analysis of movement of the free surface of the solid was not carried out to explore phenomena such as 'piling-up or sinking-in' of material around the indentation because of the relatively small field of view used in this experiment. These will be considered in the future.

While slip line fields generally provide a characterization of the deformation field at a steady state of deformation, they offer little information about the incremental development of the deformation. In contrast, the high speed image sequences and the PIV analysis offer a wealth of information pertaining to the development of the deformation. Furthermore, unlike wedge or cylinder indentation, the flat punch indentation problem is not self-similar in that the deformation evolves with increasing depth of indentation; this is an additional complication to any slip line field analysis of incipient deformation (Nepershin 2002). Nepershin (2002) has formulated an analysis of the incipient stage of deformation for plane-strain indentation with a punch. In this analysis, the velocities (hodograph) are related to the deformation of the free boundary in the sample, which in turn is a function of the depth of indentation. The analysis also suggests that a steady state of deformation is reached only when the ratio of the depth of the indentation (including material pile-up) to the width of the indenter exceeds a value of about 8, i.e. $d/b \geqslant 8$, and that only in this steady state regime is the Prandtl slip line field solution valid. A more detailed study of the deformation using the PIV approach should enable a systematic assessment of these consequences of Nepershin's analysis.

The application of PIV described herein has been restricted to an exploratory study of velocity and strain rate fields. By tracking the motion of individual particles and integrating the strain rate field along the particle trajectories, it is feasible to determine the strain field in and around the indentation zone. This has been carried out recently for large strains imposed in a specific type of sliding wedge indentation (Lee *et al* 2004, 2006). Ongoing work is implementing this path integration to obtain the strain field in indentation.

A complete determination of the parameters of the deformation field (velocity, strain rate, strain) for punch, wedge and cylinder indentation, should enable a quantitative assessment of the validity of slip line field and finite element models of indentation processes, over and above just a validation based on load–displacement data. Additional questions that may be explored, especially with advancements in the PIV technique in progress, pertain to the friction conditions at the indenter–solid

interface, concept of representative strain associated with an indentation (Tabor 1951), rotational component of plastic flow (Brown 1997), scaling of and strain gradients in the deformation field and mechanics of piling-up and sinking-in phenomena.

8. Conclusion

Direct measurement of the velocity and strain rate fields in plane-strain indentation of a semi-infinite solid by a flat punch has been demonstrated. The measurement involves the application of the technique of PIV to sequences of images of the indentation taken *in situ*. The measurement has provided a quantitative characterization of the velocity and strain rate fields in the indentation zone, the formation and evolution of regions of velocity 'discontinuity' or locally intense strain rate during the incipient and later stages of the indentation, and the variation of strain rate with indentation velocity. The magnitude of the maximum effective strain rate was $\sim$1.8 times the velocity (in mm s^{-1}) of the indentation. The measurements suggest qualitative similarity with the Prandtl slip line field solution for punch indentation of a rigid-plastic solid. The technique for the analysis of deformation is equally applicable to other types of static and dynamic indentation processes, including indentation with self-similar indenters (e.g. wedge, cylinder) and deformation processing methods. The availability of detailed data pertaining to the deformation field parameters of velocity, strain rate and strain, will enable assessments of validity of models of quasi-static indentation at an extraordinary high-level of detail. These should further our understanding of deformation phenomena in indentation, the mechanics of hardness tests, and accuracy, interpretation and scope of indentation tests.

Acknowledgments

This work was supported in part by NSF grants CMMI 0654250 and CMMI 0626047. We would like to thank the reviewers for their insightful comments and suggestions.

References

Adrian R J 1991 Particle imaging techniques for experimental fluid mechanics *Annu. Rev. Fluid Mech.* **23** 261–304

Atkins A G and Tabor D 1965 Plastic indentation in metals with cones *J. Mech. Phys. Solids* **13** 149–64

Brown L M 1997 Transition from laminar to rotational motion in plasticity *Proc. R. Soc. Lond.* A **355** 1979–90

Chaudhri M M 1993 Subsurface deformation patterns around indentations in work-hardened mild steel *Phil. Mag. Lett.* **67** 107–15

Chaudhri M M 1996 Subsurface plastic strain distribution around spherical indentations in metals *Phil. Mag.* A **74** 1213–24

Chaudhri M M and Enomoto Y (ed) 1996 *Proc. Int. Indentation Workshop (Cambridge, UK, 10–12 January 1996) Phil. Mag.* A **74** 5 (special issue)

Friedel J 1964 *Dislocations* (Oxford: Pergamon) pp 230–1

Hanemann and Schrader 1927 *Atlas Metallographicus* (Berlin: Verlag von Gebruder Borntraeger) p 760–5

Hill R, Lee E H and Tupper S J 1947 The theory of wedge indentation of ductile materials *Proc. R. Soc.* A **188** 273–89

Johnson W, Sowerby R and Haddow J B 1970 *Plane Strain Slip Line Fields: Theory and Bibliography* (Amsterdam: Elsevier)

Lee S, Hwang J, Shankar M R, Chandrasekar S and Compton W D 2004 Velocity and strain distribution in 2-D orthogonal machining *Proc. ASME Int. Mechanical Engineering Congress and Exposition (Anaheim, CA, USA, 13–19 November 2004)*

Lee S, Hwang J, Shankar M R, Chandrasekar S and Compton W D 2006 Large strain deformation field in machining *Metall. Mater. Trans.* A **37** 1633–43

Nadai A 1931 *Plasticity* (New York: McGraw-Hill)

Nepershin R I 2002 The indentation of a flat punch into a rigid-plastic half-space *J. Appl. Math. Mech.* **66** 135–40

Nguyen N T and Wereley S T 2002 *Fundamentals and Applications of Microfluidics* (Boston, MA: Artech House) pp 137–200

Nye J F 1947 Experiments on the compression of a body between rough plates *Armament Research Department (A.R.D.) Research Report No* 39/47, Division for Physical Research, Ministry of Supply, UK

O'Loughlin C D, Lehane B M and White D J 2003 Deformation patterns in sand beneath shallow foundations subjected to vertical loading *Proc. 13th Eur. Conf. on Soil Mechanics and Geotechnical Engineering (Prague, Czech Republic)* pp 767–72

Samuels L E and Mulhearn T O 1957 An experimental investigation of the deformed zone associated with indentation hardness impressions *J. Mech. Phys. Solids* **5** 125–34

Tabor D 1951 *The Hardness of Metals* (Oxford: Oxford University Press)

Tabor D 1996 Indentation hardness: fifty years on A personal view *Phil. Mag.* A **74** 1207–12

Thomsen E G, Yang C T and Kobayashi S 1965 *Mechanics of Plastic Deformation in Metal Processing* (New York: Macmillan)

White D J, Take W A and Bolton M D 2003 Soil deformation measurement using particle image velocimetry (PIV) and photogrammetry *Geotechnique* **53** 619–31

White D J and Bolton M D 2004 Displacement and strain paths during plane-strain model pile installation in sand *Geotechnique* **54** 375–97

Yew C H and Goldsmith W 1964 Stress distributions in soft metals due to static and dynamic loading *J. Appl. Mech.* **31** 636–46